

#695

METEOSAT
ENERGETIC ELECTRON DETECTOR

'88-051A-04A

Table of Contents

1. Introduction
2. Errata/Change Log
3. LINKS TO RELEVANT INFORMATION IN THE ONLINE NSSDC INFORMATION SYSTEM
4. Catalog Materials
 - a. Associated Documents
 - b. Core Catalog Materials

1. INTRODUCTION:

The documentation for this data set was originally on paper, kept in NSSDC's Data Set Catalogs (DSCs). The paper documentation in the Data Set Catalogs have been made into digital images, and then collected into a single PDF file for each Data Set Catalog. The inventory information in these DSCs is current as of July 1, 2004. This inventory information is now no longer maintained in the DSCs, but is now managed in the inventory part of the NSSDC information system. The information existing in the DSCs is now not needed for locating the data files, but we did not remove that inventory information.

The offline tape datasets have now been migrated from the original magnetic tape to Archival Information Packages (AIP's).

A prior restoration may have been done on data sets, if a requestor of this data set has questions; they should send an inquiry to the request office to see if additional information exists.

2. ERRATA/CHANGE LOG:

NOTE: Changes are made in a text box, and will show up that way when displayed on screen with a PDF reader.

When printing, special settings may be required to make the text box appear on the printed output.

Version	Date	Person	Page	Description of Change
01				
02				

3 LINKS TO RELEVANT INFORMATION IN THE ONLINE NSSDC INFORMATION SYSTEM:

<http://nssdc.gsfc.nasa.gov/nmc/>

[NOTE: This link will take you to the main page of the NSSDC Master Catalog. There you will be able to perform searches to find additional information]

4. CATALOG MATERIALS:

- a. Associated Documents To find associated documents you will need to know the document ID number and then click here.
<http://nssdcftp.gsfc.nasa.gov/miscellaneous/documents/>

- b. Core Catalog Materials

REQ. AGENT

JLJ

RAND NO.

METEOSAT

ACQ. AGENT

HKH

ENERGETIC ELECTRON DETECTOR

88-051A-04A SPMS-00566

THIS DATA SET CATALOG CONSISTS OF 1 TAPE. THE TAPE IS A 9-TRACK, 6250 BPI, BINARY, LABELLED AND CREATED ON A VAX COMPUTER. THE D AND C NUMBERS AND TIME SPANS ARE AS FOLLOWS:

D#	C#	FILES*	TIME SPANS
---	---	-----	-----
D-80282	C-27620	90	06/22/88 - 08/31/89

*30 DATA FILES. THE REST ARE HEADER AND TRAILER FILES.

88-051A-04A

MULLARD SPACE SCIENCE LABORATORY
DEPARTMENT OF PHYSICS AND ASTRONOMY
UNIVERSITY COLLEGE LONDON

Holmbury St. Mary
Dorking
Surrey
RH5 6NT

Tel (0483) 274111
Telex 859185 UCMSSL G
Fax (0483) 278312

January 25, 1990

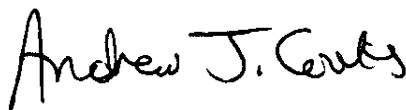
Dr Joe King,
Code 633,
National Space Science Data Center,
NASA/Goddard Space Flight Center,
Greenbelt,
Maryland 20771,
USA

Dear Dr King,

ESA have agreed that we can send you the Meteosat SEM-2 data. I enclose a tape we have produced which includes fluxes covering the period June 88-Aug 89, together with documentation on how to read the tape. I hope you can read it successfully.

We are still processing the data and will be pleased to send you more in the Fall.

Yours sincerely,



Dr A.J. Coates

Meteosat Archive Tape Specification

①

The tapes will consist of files of the form:

- (1) JUN89_ARCHIVE_HR.DAT - This contains the high resolution data.
- (2) JUN89_ARCHIVE_LR.DAT - This contains the low resolution data.

Each of these 2 files will be written for each month of Meteosat P2 data, by the program [MAB.METEOSAT.P2]ARCHIVE_METEOSAT_P2.EXE, and the input to this program is the disk file produced by H.E.Huckle's programs: MONTH3_P2.EXE, MONTH2_P2.EXE on [HEH.METEOSAT.P2].

The files will be written to disk using the following open and write statements. All variables are real*4 .

```

      open( unit      = lun_high,
&         name       = archive_file(1),
&         status     = 'new',
&         access     = 'direct',
&         recl       = 96,
&         form       = 'unformatted',
&         recordtype = 'fixed' )

      do i = 1, num_hr_values
      !
      !           WRITE THE DATA TO THE HIGH RESOLUTION ARCHIVE FILE.
      !           -----
      !
      write( lun_high' i )
&         xb_hr(i),
&         xt_hr(i),
&         total_flux_hr(i),
&         y_e10_hr(i),
&         y_e21_hr(i),
&         y_e32_hr(i),
&         y_e43_hr(i),
&         y_e54_hr(i),
&         spectral_index_hr(i),
&         delta_spectral_hr(i),
&         ( polar_flow_hr(j,i), j = 1, 5),
&         ( azim_flow_hr(iaz,i), iaz = 0, 5),
&         ( ( polar_azim_flux_hr(k,j,i), k = 0, 5 ), j = 1, 5 ),
&         c_e10_hr(i),
&         c_e21_hr(i),
&         c_e32_hr(i),
&         c_e43_hr(i),
&         c_e54_hr(i),
&         ( ( polar_azim_counts_hr(k,j,i), k = 0, 5 ), j = 1, 5 ),
&         anistropy_hr(i),
&         thetapole_hr(i),
&         phipole_hr(i),
&         kpno_hr(i),
&         kpvalue_hr(i),
&         latch_hr(i),
&         ( zone_hr(k,i), k = 1, 4 )

      enddo

      close( unit = lun_high )

      open( unit      = lun_low,

```

```

&      status      - 'new',
&      access      - 'direct',
&      recl        - 96,
&      form        - 'unformatted',
&      recordtype  - 'fixed' )

```

```

do i = 1, num_lr_values
!
!      WRITE THE DATA TO THE LOW RESOLUTION ARCHIVE FILE.
!      -----
!
write( lun_low' i, iostat = iok )
&      xb_lr(i),
&      xt_lr(i),
&      total_flux_lr(i),
&      y_e10_lr(i),
&      y_e21_lr(i),
&      y_e32_lr(i),
&      y_e43_lr(i),
&      y_e54_lr(i),
&      spectral_index_lr(i),
&      delta_spectral_lr(i),
&      ( polar_flow_lr(j,i), j = 1, 5),
&      ( azim_flow_lr(iaz,i), iaz = 0, 5),
&      ( ( polar_azim_flux_lr(k,j,i), k = 0, 5 ), j = 1, 5 ),
&      c_e10_lr(i),
&      c_e21_lr(i),
&      c_e32_lr(i),
&      c_e43_lr(i),
&      c_e54_lr(i),
&      ( ( polar_azim_counts_lr(k,j,i), k = 0, 5 ), j = 1, 5 ),
&      anistropy_lr(i),
&      thetapole_lr(i),
&      phipole_lr(i),
&      kpno_lr(i),
&      kpvalue_lr(i),
&      latch_lr(i),
&      ( zone_lr(k,i), k = 1, 4 )

enddo

close( unit = lun_low )

```

These items being the following:

Monthly High Time Resolution Files

These will have time resolution of 500, 500 and 600 seconds. The parameters to be included are:

Start Time	(1)
End Time	(1)
Total Flux	(1)
Flux(E)	(5)
Spectral Index	(1)
Error Bar of Spectrum	(1)
Polar Flow	(5)
Azimuthal Flow	(6)
Polar-Azim Flux	(5,6)
Counts(E)	(5)
Polar-Azim Counts	(5,6)
Anistropy	(1)

```

theta          (1)
phi            (1)
Kp             (1)
Kp(tau)       (1)
MUM           (5) recognize startup pattern and
                set to zero before adding

```

Monthly Low Time Resolution Files

These will have time resolution of 30 minutes. The parameters to be included are the same as the high time resolution files. Except for the MUM which is a sum. All the others are averages:

The data contains 48 thirty minute bins per day, with the first bin starting at midnight. If any of these periods contains no data all the data values are set to -1's.

```

Start Time      (1)
End Time        (1)
Total Flux      (1)
Flux(E)         (5)
Spectral Index   (1) average distribution before calculating
Error Bar of Spectrum (1)
Polar Flow      (5)
Azimuthal Flow  (6)
Polar-Azim Flux (5,6)
Counts(E)       (5)
Polar-Azim Counts (5,6)
Anisotropy      (1) average result after calculating
theta           (1) "
phi             (1) "
Kp              (1)
Kp(tau)        (1)
MUM            (5) recognize startup pattern and
                set to zero before adding

```

All the files will then simply copied to tape, using the following commands:

```

$!
$ allocate mfa0:
$ ini      mfa0: metp2 / dens = 6250 / override = owner_identifier
$ mount   mfa0: metp2 / dens = 6250 / override = owner_identifier
$ copy *.* mfa0:[]*.*
$ dismount mfa0:
$ dealloc mfa0:
$!

```

Quest for the source of Meteosat anomalies

A.J.Coates, A.D.Johnstone, D.J.Rodgers

Mullard Space Science Laboratory, University College London,
Holmbury St Mary, Dorking, Surrey RH5 6NT, UK

G.L.Wrenn, A.J.Sims

Space Departmentt, Royal Aerospace Establishment,
Farnborough, Hants GU14 6TD, UK

Abstract

Three ESA Meteosat geostationary satellites have suffered from a series of anomalies which disturb routine operations; most commonly, the scan of the radiometer has stopped or jumped requiring a reset command to be sent.

Experience with Meteosat-F1 launched in 1977 (Robbins, 1979) prompted the installation of an AFGL electron spectrometer (50eV-20keV) on Meteosat-F2, in an attempt to demonstrate a direct link between the anomalies and surface charging. Data spanning August 1981 to March 1987 have provided interesting evidence for differential charging (Wrenn and Johnstone, 1987) and permit the establishment of an empirical model of charging fluxes through a solar cycle. However, the reported anomalies do not fit the pattern for surface charging effects and no real link was found. Deep dielectric charging has now become the most likely explanation and consequently Meteosat-P2, launched in June 1988, carries a LANL monitor of 43-300 keV electrons.

The Meteosat anomaly chronicle is the result of reliable recording procedures at ESOC and it represents a unique data base for an important class of ESD effects which occur at Geosynchronous orbit. This paper gives some preliminary results from Meteosat P2 and attempts to assess their relevance within the context of earlier conclusions from the Meteosat-F2 studies.

INTRODUCTION

Since Meteosat-F1 suffered many operational anomalies it was decided to include a spacecraft charging monitor on F2 to see whether the anomalies were related to spacecraft surface charging. While that experiment certainly showed strong evidence of charging on F2 there was no correlation with the occurrence of unexplained anomalies, which were also present on F2. The decision was then made to investigate the higher energy range of electrons associated with deep dielectric charging. Thus SEM-2 was commissioned to study the 30-300keV range of electrons.

The sensor unit was provided by Los Alamos National Laboratory, USA as a spare Lo-E sensor [Aiello et al., 1975] from other programmes, to the Mullard Space Science Laboratory of University College London (MSSL) which provided the power supplies, data processing unit and interface to the Meteosat spacecraft. MSSL was further responsible for integration, testing and calibration of the instrument, and delivery of the instrument to the spacecraft. MSSL also provided a memory upset monitor (MUM) in this instrument, as requested by ESA.

This paper describes briefly the history of the F1 and F2 studies, in particular the role of spacecraft charging in generating the anomalies and the possibility of deep dielectric charging as an explanation. We then go on to a description of the SEM-2 instrument, and the conversion of the observed counts to physical units. Typical natural events in the spacecraft environment as seen by SEM-2 are shown. The correlation of the energetic electron fluxes to the occurrence of anomalies, which on P2 occur at a rate which is about four times that of F2, are the major results. As data have accumulated we have been able to show a striking correlation between the energetic electron fluxes and the spacecraft anomalies. For the first time it appears that the measurements provide a good indication of anomalies.

1 Meteosat operational anomalies and spacecraft charging

1.1 Meteosat-F1

When Meteosat-F1 was launched in 1977 many operational anomalies occurred (about 150 in 3 years) for which there was no immediate explanation. However, their occurrence was related to geophysical factors outside the normal realm of spacecraft engineering, namely that they were more likely when there was strong geomagnetic

activity and they exhibited a tendency to occur at certain times of day [Robbins, 1979]. It had recently been discovered then that geosynchronous spacecraft could charge up to many thousands of Volts [deForest, 1972] in the ambient plasma so it was natural to attribute the anomalies to charging, or more precisely to differential charging. Unless the complete outer surface of the spacecraft is conductive and electrically connected, it is normal for different parts of the spacecraft to charge to different voltages. At times, adjacent surfaces can be more than a thousand volts apart. This in turn leads to arcing between the surfaces and results in large electrical transients in the spacecraft harness. After the problems were encountered by Meteosat-F1 a series of laboratory tests was carried out which demonstrated that arcing occurred if the spacecraft was illuminated by an electron beam, and that electrical transients could induce anomalous behaviour. It was not possible to simulate in-orbit conditions completely and thus it was not possible to establish the causal chain completely.

1.2 Meteosat-F2

Before the second spacecraft Meteosat-F2 was launched some changes were made to reduce the susceptibility to differential charging, namely grounding of thermal shields and hardening of some critical electrical interfaces, and to include two charging monitors to complete the link between the anomalies and spacecraft charging. One of the monitors was designed to detect arcing transients on a short antenna within the spacecraft. In flight no such events were detected, but it is not known whether the instrument was sensitive enough, or whether it was not operating correctly or whether there were no significant transients. Therefore we can say no more about it. The second monitor measured the ambient plasma electrons in the energy range 50eV to 20KeV and therefore could measure the charging current directly. Not only that but it was anticipated that in the event of spacecraft charging the energy spectrum would be modified in a manner which would allow the spacecraft potential to be measured. Briefly, the objective of the instrument was to see if the anomalies occurred when the spacecraft was charged. The results of this investigation have been published in a number of reports [Johnstone et al, 1985, Wrenn and Johnstone, 1987]. Although no direct link between differential charging and anomalies was found there were several interesting and significant (for this problem) findings which we summarize here.

1. Two types of differential charging were observed. One type occurred during eclipses and had been expected. The second type, called a "barrier event", only occurred when the radiometer mirror was completely in shadow and was therefore probably because the mirror was charging up. The two types are illustrated in Figures 1 and 2 and explained in the figure captions.
2. A charging index based on an estimate of the net electron flux to the spacecraft (incident electrons minus secondary emitted electrons) was 95 percent successful in predicting whether the spacecraft would charge up in any particular eclipse.
3. There was an indication in the electron spectrum during eclipse charging that the voltages in differential charging were limited by discharging currents of secondary electrons from one part of the spacecraft to another.
4. Only one anomaly, in more than 100, occurred at any time near an observable differential charging event. In all cases there was no evidence that the spacecraft was charged to more than a few volts.
5. The anomalies attributed for lack of a better cause to arcing did, as before on Meteosat-F1, show a dependence on geophysical parameters, ie local time, solar aspect angle and geomagnetic activity [see Figure 3].
6. When separated into four types of anomaly the solar aspect angle, and local time dependence was different for all four groups.
7. The most common type of anomaly, the radiometer stoppage or position jump was most common at the equinox and was associated with a period of sustained high geomagnetic activity.

The conclusions of the analysis were that the anomalies were not the result of differential charging but that they were caused by some external geophysical effect. The four types of anomaly were caused by four different mechanisms.

Frezet et al [1989] have made an analysis of the charging of Meteosat with the NASCAP charging analysis code. They find that the differential voltages developed are greater at equinox and suggest that this is the explanation for the occurrence of radiometer anomalies at this time. The charging levels they obtain are many thousands of volts. However the only differential charging of the radiometer is observed away from equinox, when the radiometer mirror is totally in shadow. Also

when anomalies occur there is no evidence of any charging. Finally Frezet et al only developed such a charging scenario when extreme plasma conditions are used and such extreme conditions were not observed by the monitors on Meteosat-F2 itself.

We were left with the situation that we still do not know what caused the anomalies on Meteosat-F1 or F2. Spacecraft surface charging, or differential charging, appears to be ruled out. In their final report Johnstone et al [1985] suggested that it might be caused by penetrating electrons producing deep dielectric charging. This was partly based on the observation that a sustained period of high geomagnetic activity was required to develop the effect, and that the trapped energetic electrons are known to be slower to respond to geomagnetic activity than the plasma at energies of less than 20KeV. Therefore it was suggested that the third Meteosat flight should carry a detector of more energetic electrons. Accordingly it was decided to include in the payload the SEM-2 detector which measures the energy and angular distribution of electrons in the energy range 30KeV to 300KeV.

The behaviour of electrons above 30keV at Geosynchronous orbit has been studied by the Los Alamos group [Baker et al, 1981]. In Figure 4 the average fluxes for the whole of 1977 and 1978 are compared to the particles' range in aluminium as calculated by the SHIELDOSE program: this shows that higher energy particles can penetrate appreciable distances before being stopped. To penetrate 0.5mm into polythene, an electron requires an energy of 200KeV (see Figure 5 from Powers et al. [1981]). Deep dielectric charging, where penetrating electron fluxes may cause buildup of charge and eventual breakdown in insulators, has been postulated as the reason for anomalies on other spacecraft [eg Baker et al, 1986].

2 Instrumentation

The measurement of electrons above 30 keV implies a different type of sensor to the F2 instrument, which consisted of two electrostatic energy analyser/channeltron combinations, giving differential energy measurements. The standard technique for tens to hundreds of keV particles has become the surface barrier solid-state detector [eg Aiello et al, 1975]. Using electronic thresholds this technique also gives differential energy measurements.

SEM-2 contains five surface barrier detector-collimator systems, arranged to accept particles from 5 different angular ranges. The 5 ranges are of spacecraft polar angle: azimuthal angle measurements are achieved by timing. Each of the detectors

the Goddard spaceflight center and are as follows:

Energy level	E_{min} (keV)
E5	42.9
E4	59.4
E3	90.7
E2	134.9
E1	201.8

Table 1: Lower level discriminator settings for SEM-2

Full details of the operation of the instrument are given in the final report to ESA (Coates et al, 1989). Here we restrict ourselves to a description of the information transmitted.

A transmission list is accumulated in 4 formats, approx 100 seconds. A complete experiment cycle takes 500 or 600 seconds since one polar angle is sampled in each 4-format cycle. The raw parameters received on the ground are as follows, every 100 seconds.

- A 5-point energy spectrum, compressed counts E1-E5, for a particular polar angle, summed over azimuth.
- A 6-point azimuth array, compressed counts A1-A6, for a particular polar angle, summed over energy.
- Overflow information as appropriate for each of the above bins.
- Timing information to relate azimuth to spin phase.
- Synchronisation information for data checking.
- MUM parameters on SEU and latch-up.

Counts are converted to flux and plotted. The principal result of the data processing was the provision of summary plots of the data from SEM-2. It is essential that users of the SEM-2 data be able to tell from the plots alone, the general behaviour of the plasma environment at all times and be able to identify times of particular interest. To enable this, the plots contain parameters that summarise the data, parameters that interpret the data further and associated parameters for comparison. This led to the choice of eight panels of data presented on a single page with one page per day; an example is shown in Figure 6. These panels are:

Total Flux; Flux; Spectral Index; Polar Flow; Azimuthal Flow; Anisotropy Index and axis of symmetry; Kp; MUM and Latch-up.

2.1 Total Flux

Total flux of electrons within the energy range of the detector (42.9-300keV) and summed over all polar and azimuthal bins.

2.2 Flux

This is the Flux (expressed as a grey scale level) in the 5 energy bands of the analyser, from 43 to 300KeV. These energy bands are: 42.9 to 59.4KeV, 59.4 to 90.7KeV, 90.7 to 134.9KeV, 134.9 to 201.8KeV, 201.8 to 300(nominal)KeV. These data are summed over all polar and azimuthal angle bins.

The analyser returns integral measurements of counts versus energy. Counts are measured as the energy cut-off or threshold of the instrument is progressively raised. To calculate the counts in one energy band, the counts measured with the cut-off at the top and bottom of that band are subtracted.

2.3 Spectral Index

This index determines the 'hardness', or shape of the energy spectrum. This is generally negative because, except in extraordinary cases, there are less particles at high energy than at low energy. The index is simply the slope of the log of the energy spectrum.

2.4 Polar Flow

This is the flux (expressed as a grey scale) in the 5 polar angle sectors of the analyser. These sectors look in the polar directions 30°, 60°, 90°, 120° and 150° to the spacecraft spin axis. The spacecraft spin axis is to a good approximation parallel to the Earth's spin axis. The angle bins cover a nominal $\pm 5^\circ$.

2.5 Azimuthal Flow

This is the flux (expressed as a grey scale) in the 6 azimuthal angle sectors of the analyser. These sectors cover the angles 0° to 60°, 60° to 120°, 120° to 180°, 180° to 240°, 240° to 300° and 300° to 360°, in spacecraft coordinates. Note that at 0° the analyser looks towards the sun.

The anisotropy index describes the angular shape of the plasma distribution relative to its axis of symmetry, shown as theta and phi. A trapped particle distribution is a 'pancaked' i.e. enhanced perpendicular to the magnetic field compared to along it. Where plasma is newly injected it tends to lie along the field line in a 'cigar-shaped' distribution. The index is positive for pancaked distributions and negative for cigar-shaped distributions. The anisotropy index is calculated [using techniques adapted from Sanderson and Page, 1974, Sanderson and Hynds, 1977, Higbie and Moomey, 1977] by fitting the data to a set of spherical harmonics. Since we believe that the magnetic field organizes the plasma, then the axis of symmetry represents the magnetic field direction. However, it does not distinguish between positive and negative field directions.

2.7 K_p and $K_p(\tau)$

K_p is an index of planetary magnetospheric activity for the whole of Earth, in a three hour period. In the monthly plots, $K_p(\tau)$ is plotted. This is a weighted average of successive K_p values and was devised by Wrenn [1987]. Many magnetospheric processes are more dependent on the general level of magnetospheric activity in the recent past than on the present level. Wrenn showed that anomalies on Meteosat-F2 was better correlated with an appropriately time-averaged activity index than with the real-time index.

2.8 MUM

The Memory Upset Monitor results are displayed as lines in the bottom panel. These display the number of 'single-event upsets' i.e. errors found in a known memory pattern, in the 4 memory zones of the test RAM. A test pattern is seen in the plot when the instrument is first powered on. A fifth line in this plot shows the occurrence of 'Latch-ups' where the test RAM attempts to draw excessive current. This line can take only values 1 - Latch-up and 0 - no latch-up.

3 Typical events

To illustrate the environment at Geosynchronous orbit as seen by Meteosat-F2 SEM-2 we include some data examples.

27th June 88 (Figure 6): On the dayside, eg at 1300Z, a "pancake" distribution is seen in the polar angle plot where fluxes are peaked at the equator: this is typical for a trapped electron distribution diffusing into the loss cone. At approximately 0200Z there is a typical isolated, injection event which shows some important features. First the total flux drops by two orders of magnitude, relatively slowly. Then it increases sharply to a level greater than before. Finally it decreases slowly to the initial level.

In Figure 7 we have looked at the results from 4 satellites simultaneously to the injection in Figure 6. Local time around the Earth is seen in the small inset diagram; spacecraft 1 and 2 (Meteosat) see the injection, while 3 and 4 show velocity dispersion with higher energy electrons arriving first.

The monthly summary example in Figure 8 shows the wider view of the dramatic events during March 1989. The spacecraft was outside the magnetopause for significant times on March 13 since the magnetosphere was severely compressed at that time.

4 Meteosat anomaly correlations

When comparing the occurrence of anomalies with the results from SEM-2 on a monthly basis it soon became apparent that anomalies, particularly radiometer anomalies, nearly always occurred when the flux of energetic electrons was high. The problem then becomes to verify such an association statistically and then to try and determine a causal link. While we have been able to achieve the former, the latter is still some way from a satisfactory conclusion. In other words there is no doubt that anomalies and high energetic electron fluxes are linked but we do not yet know if the energetic electrons cause anomalies and if they do, how they do. Alternatively the high electron fluxes may themselves be the consequence of another agent which is the actual cause of the anomalies.

A plot of the anomalies we have used in this study is given in Figure 9, where we have organized the anomalies as follows:

RPJ	Radiometer position jump
RDS	Radiometer stoppage
RGC	Radiometer gain change
BAT	Battery anomaly
SIC	SIC anomaly
OTH	Other anomaly

RDS is by far the most frequent type of anomaly.

First we establish that the radiometer anomalies show the same systematic behaviour as on the previous Meteosat flight models. Figure 9 shows the local time and annual distribution for the 76 unexplained anomalies seen in the first year. They are essentially identical with distributions obtained for F2. In local time the peak occurrence is in the period 02 to 05 local time but there is a non-negligible rate of occurrence throughout the day. This distribution is reminiscent of the distribution of a type of charging event on Meteosat-F2 which were called barrier events [Johnstone et al, 1985]. However none of the Meteosat-F2 anomalies was concurrent with a barrier event. Anomalies are, as with F2, are most likely at the equinoxes and least likely at the solstices. This demonstrates once again essentially a dependence on solar aspect angle. The main conclusion we wish to draw from this diagram is that the radiometer anomalies are caused by the same mechanism as on Meteosat-F2. It is interesting to note that the anomaly rate is approximately 4 times that of F2, which suffered 80 anomalies in 4 years.

In the next series of plots the statistics of the average daily flux is examined. Figure 10 is a histogram of the number of days in the year a particular value of the daily average flux was recorded. For example the column labelled 7 contains number of days the average fluxes were in the range 7000 to 7999. Thus this graph if normalized would show the probability that the average flux has a particular value. It could be used for example to calculate the amount of radiation a geosynchronous satellite would encounter. Figure 11 shows the yearly total number of anomalies which occurred on days with that average daily flux. Compared with the distribution of Figure 10 it is clearly strongly biased towards the higher fluxes. By dividing the distribution of Figure 11 by that in Figure 10 we calculate the average number of anomalies in a day if the average flux has the given value. This produces the very striking distribution shown in Figure 12. Once the flux exceeds 19000 the average daily rate is greater than one. This can be interpreted as the probability of an anomaly in given flux conditions. It is the first time we have achieved a connection between a characteristic of the plasma environment and the occurrence of anomalies. No such connection was found between the low energy plasma ($E < 20$ KeV) environment and anomalies on Meteosat-F2.

This does not yet establish a causal connection because the high fluxes could be caused by the same unknown phenomenon which causes the anomaly. What about the annual variation in the occurrence? This could arise because the

electron fluxes have a similar annual variation. In figure 10 the mean monthly flux (dotted line) is plotted with the monthly number of anomalies. Both show a peak in March and April which were two of the most active months magnetically for a long time. In Sept and Oct where the anomaly rate peaks the monthly mean flux actually has its minimum value for the year. This suggests that there are at least two independent factors responsible for radiometer anomalies; one is associated with high fluxes of energetic electrons fluxes, and the other with the solar aspect angle.

It is possible that there is a third factor, which we see in the form of the local time variation of anomalies. This is likely however to be linked to a local time variation in the energetic electron fluxes. We have not been able to test this hypothesis yet because of the need to develop some specialised software to access this aspect of the data.

These results give us a positive result on the cause of anomalies for the first time. It is difficult to achieve a better level of proof without having a clearer idea of the mechanism which will allow us to develop a physical model which can be directly tested. An attempt to do this based on deep dielectric charging will form the next stage of our investigation.

The interaction between Meteosat and the environment is clearly a very complex one which we do not yet understand. Although spacecraft charging is significant, and needs to be minimized as we have now learned, there are other things going on for which we have not yet found the appropriate ameliorative methods.

Clearly the investigation should continue. Ideas of such effects as deep dielectric charging are still vague and need to be sharpened. This may require laboratory testing to try to replicate the phenomena, and the development of physical models which can be tested against the observations. There is also still a need to observe in more detail the interaction of a spacecraft with its environment and over a wide range of energies.

5 Summary of results

- Unexplained anomalies on Meteosat-P2 have continued at a rate about 4 times higher than that observed on F2. The P2 and F2 anomalies show a similar local time and seasonal dependence.
- The anomalies show a good correlation with electron fluxes in the range 43-300keV. This is the first time that a correlation of anomalies has been demon-

strated with the Meteosat in-situ environment monitor data - the charging instrument on F2 saw charging events but they did not correlate with anomalies. Taken on its own the P2 correlation would confirm deep dielectric charging as a possible mechanism.

- However the seasonal dependence of anomalies, which strongly peak at equinox, show that at least one additional process is at work.
- We still maintain that spacecraft charging cannot explain the observed Meteosat anomalies, although it should still be minimised to avoid others.

6 Further study

Future study will be pursued on the following items:

- Processing of further SEM-2 data (already underway at MSSL).
- An explanation should be sought for the seasonal variation of anomalies on Meteosat.
- Further study is needed on the deep dielectric charging mechanism.
- Further effort should be put into calculating dose rates and penetration depths from the SEM-2 data.
- Further instruments should be included on future spacecraft, not only Meteosat, to look at both charging and deep dielectric effects. For the Meteosat series, higher energy electrons measurements extending up to 1MeV are encouraged to study the deep dielectric charging in more detail.

ACKNOWLEDGEMENTS

Most of this work was performed as part of ESA contract 7879/88/F/TB. The SEM-2 sensor head was provided by Los Alamos National laboratory, thanks are due to R.Belian and W.Aiello. T.A.Fritz made a new unit available when launch delays caused calibration and noise problems; he also provided the Los Alamos data shown in Figure 7. Calibration was done at NASA-Goddard Spaceflight Center: S.Brown and C.Smith are gratefully acknowledged. The interest, help and patience of the ESA Meteosat project team, principally J.Aasted, was much appreciated particularly regarding installation of the new sensor head.

- Aiello, W.P., Belian, R.D., Conner, J.P., Higbie, P.R., Martin, W.B. & Singer, S., "An energetic particle detector for a synchronous satellite", *IEEE Trans Nucl Sci*, NS-22, 575, 1975.
- Baker, D.N., Belian, R.D., Higbie, P.R., Klebsadel, R.W. and Blake, J.B., "Deep dielectric charging effects due to high energy electrons in Earth's outer magnetosphere", submitted to *J.Electrostatics*, 1986.
- Baker, D.N., Higbie, P.R., Belian, R.D., Aiello, W.P., Hones, E.W., Jr., Tech, E.R., Halbig, M.F., Payne, J.B., Robinson, R. and Kedge, S., "The Los Alamos Geostationary Orbit Synoptic Data Set: a compilation of energetic particle data", *Los Alamos report LA-8843*, 1981.
- Coates, A.J., Johnstone, A.D., Rodgers, D.J and Huckle, H.E., "SEM-2 data processing 22 June 1988 to 30 June 1989", report on ESA contract 7879/88/F/TB, 1989.
- DeForest, S.E., "Spacecraft charging at synchronous orbit", *J.Geophys.Res.*, 77, p651, 1972.
- Frezet, M., Daly, E.J., Granger, J.P and Hamelin, J., "Assessment of electrostatic charging of satellites in the geostationary environment", *ESA Journal*, 13, 89-117, 1989.
- Higbie P.R. and Moomey W.R. "Pitch Angle Measurements from Satellites Using Particle Telescopes with Multiple View Directions", *Nucl. Instrum Methods*, 146 p.439, 1977.
- Johnstone A.D., Wrenn G.L., Huckle H.E. and Scott R.F. "Meteosat-F2 Spacecraft Charging Monitors", Final Report ESA contracts 4715/81/F/CG, 5911/84/F/CG, 1985.
- Powers W.L., Adams B.F. and Inouye G.T. "Electron Penetration of Spacecraft Thermal Insulation", *Spacecraft Charging Technology 1980*, AFGL-TR-81-0270, p.86, 1981.

Robbins,A., "Meteosat spacecraft charging investigations", final report, ESA contract 3561/78F/CG/SC, 1979.

Sanderson T.R. and Hynds R.J. "Multiple Telescope Measurements of Particle Anisotropies in Space", *Planet. Space Sci.*, **25** p.799, 1977.

Sanderson T.R. and Page D.E. "Spherical Harmonic Analysis of Satellite Anisotropy Measurements", *Nucl. Instrum. Methods*, **119**, p.177, 1974.

Wrenn G.L., "Time-Weighted Accumulations $ap(\tau)$ and $Kp(\tau)$ ", *J. Geophys. Res.*, **92**, no. A9, p.10125, 1987.

Wrenn, G.L. and Johnstone, A.D., "Evidence for differential charging on Meteosat-2", *J.Electrostatics*, **20**, 59-84, 1987.

8 Figure captions

Figure 1 - An eclipse charging event seen by the F2 experiment. From the change in the energy spectrum it is inferred that the potential of the whole satellite went 5kV negative relative to space in this eclipse. The rising peak is due to differential charging of another part of the spacecraft at an even more negative potential (up to 600V more negative). [from Johnstone et al, 1985].

Figure 2 - Example of a "barrier event" on F2. This is where part of the spacecraft, electrically isolated from the rest, is shadowed and charges negatively as the whole spacecraft does in eclipse. High potential differences between adjacent parts of the spacecraft may then result in arcing. The low energy electrons observed in the event are due to reflection by the potential barrier of photo- and secondary electrons back to the spacecraft. While these events were correlated with radiometer mirror shadowing they were not correlated with observed anomalies. [from Johnstone et al, 1985].

Figure 3 - Distribution of F2 anomalies in local time and season [from Wrenn, 1989].

Figure 4 - Average electron flux spectra averaged over the 2 years 1977 and 1978. 90% of the samples are below the top curve and above the bottom curve. Mean electron ranges are also plotted. [fluxes from Baker et al, 1981, range from SHIELDOSE code developed by Seltzer (NBS 1116)]

Figure 5 - Electron range in polyethylene [from Powers et al, 1981]

Figure 6 - Daily plot for 27 June 88 showing an injection event at 0220Z.

Figure 7 - Energetic electron measurements from various positions at Geosynchronous orbit around the earth (see inset), showing the 27 June injection on spacecraft 1 and 2 (Meteosat) and velocity dispersion effects on 3 and 4. 1,3,4 are US spacecraft, those data courtesy LANL.

Figure 8 - Monthly plot for March 89

Figure 9 - All P2 anomalies as a function of local time and date

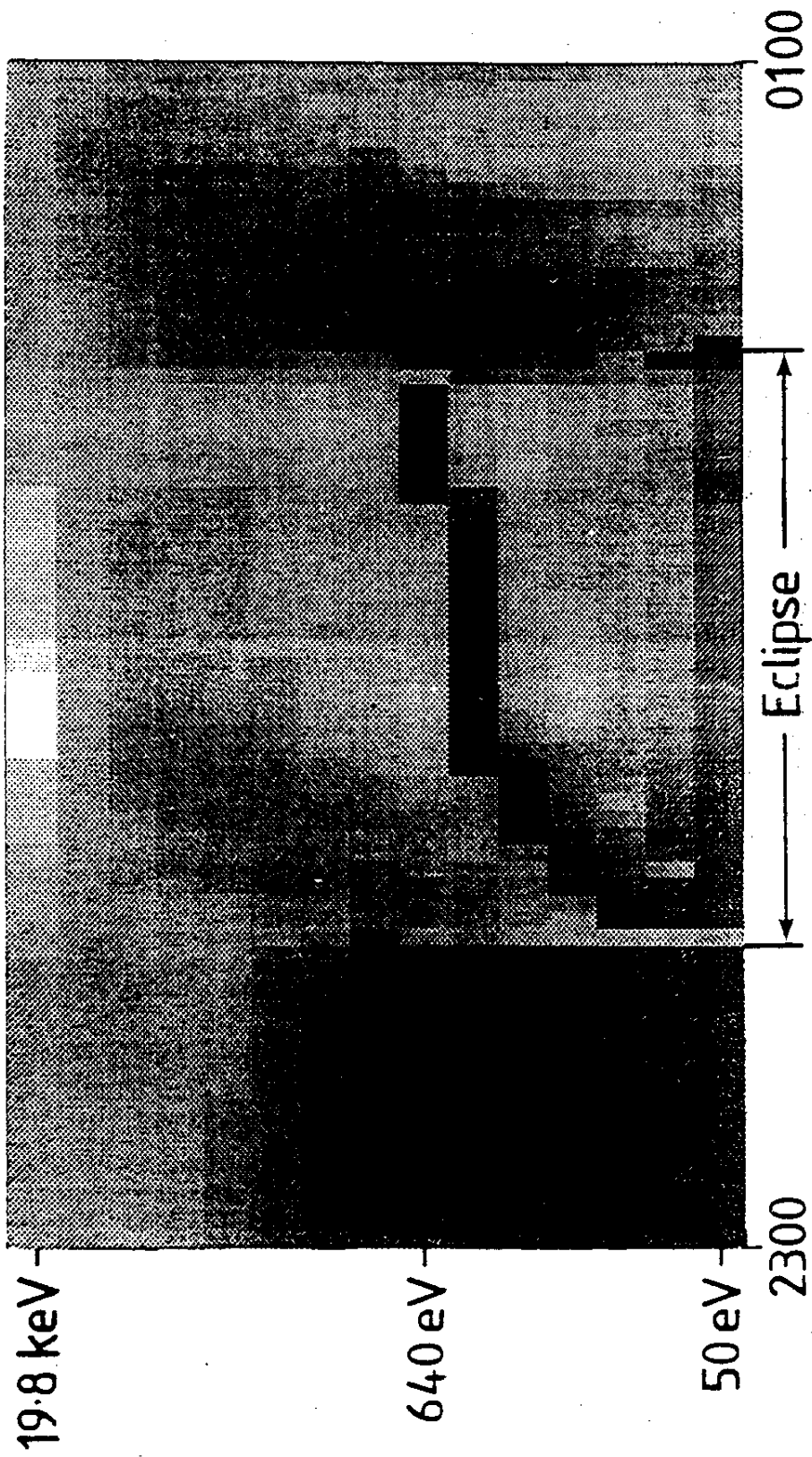
Figure 10 - Number of days with given average flux (thousands of flux units)

Figure 11 - Anomalies as a function of daily flux

Figure 12 - Average daily anomaly rate (anomaly probability) as a function of daily flux

Figure 13 - Anomalies (solid line) and monthly mean flux (dotted line for different months)

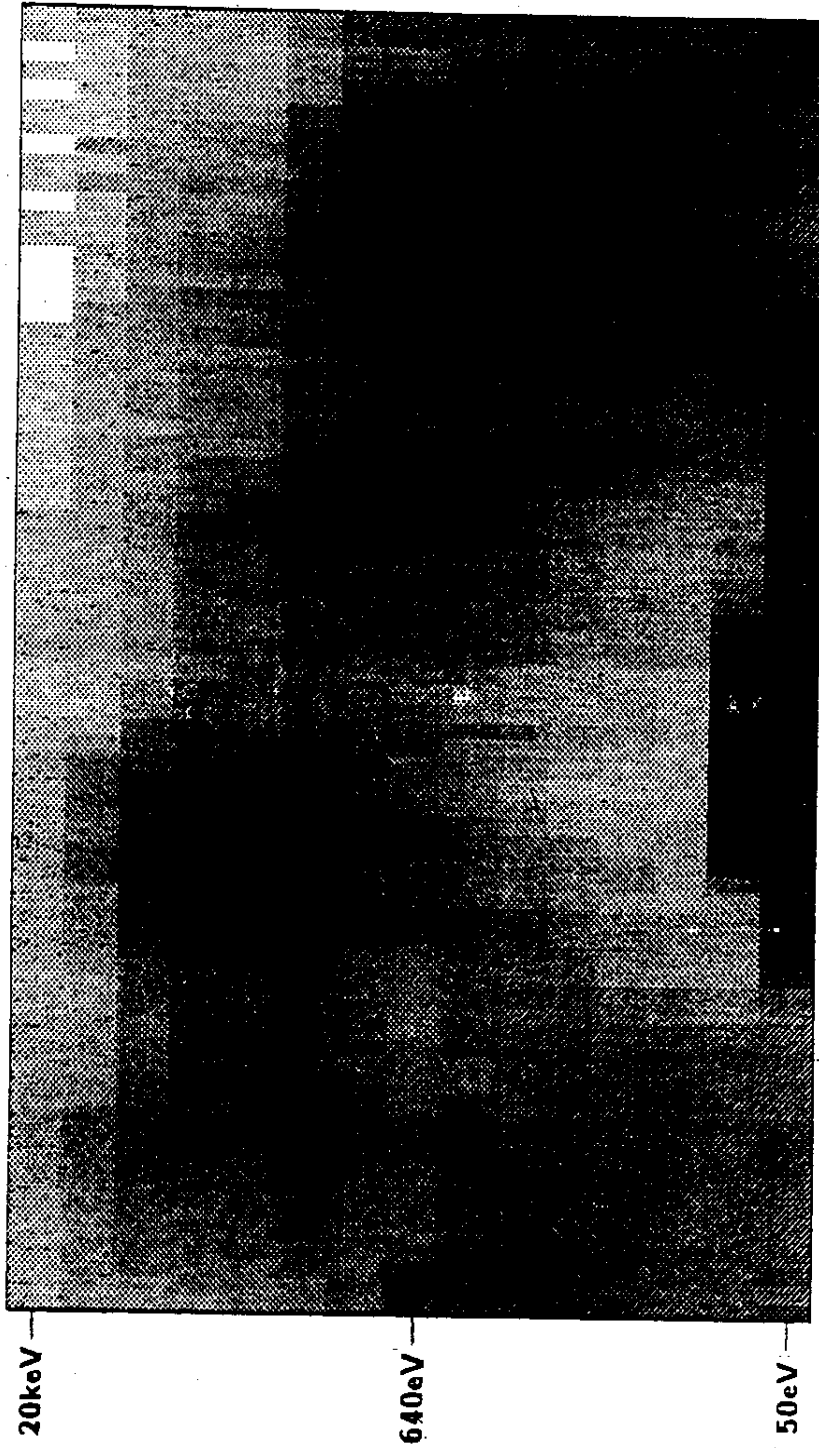
Meteosat F2, SSJ/3 Data 3/4 April 1982



U.T.

FIG 1

METEOSAT F2, SSJ/3 DATA
STARTING AT 3 1 41.8 ON 25/ 7/82

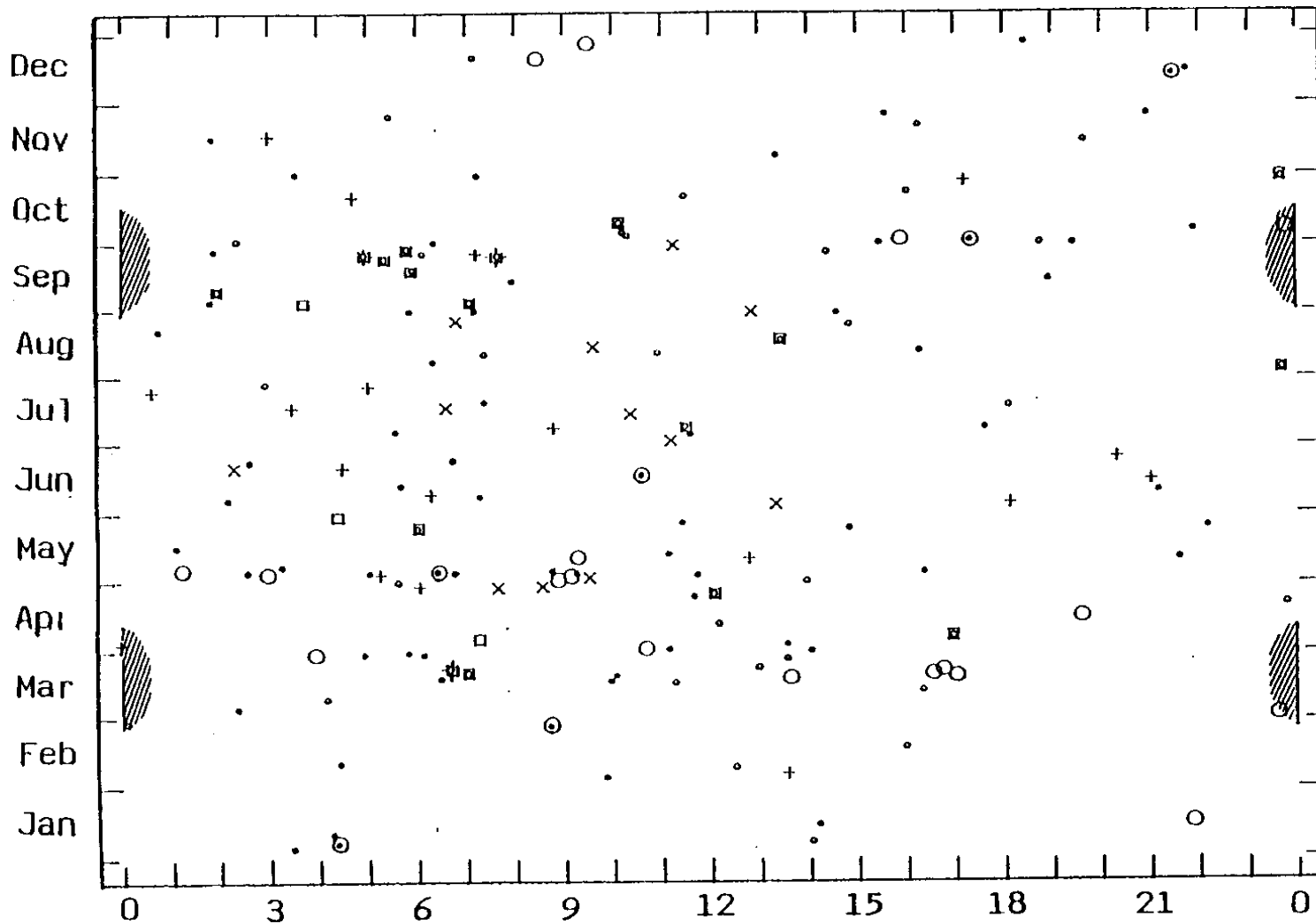


← Barrier Event →

2 HOURS

FIG 2

METEOSAT ANOMALIES (1981-85)



LOCAL TIME (h)

	METEOSAT-1	METEOSAT-2
RADIometer	•	◦
CALibration		◻
Power SS/BAT	○	×
AOCS/SIC		+

FIG 3

ENERGETIC ELECTRON FLUX and RANGE ALL LOCAL TIMES, 1977 & 1978

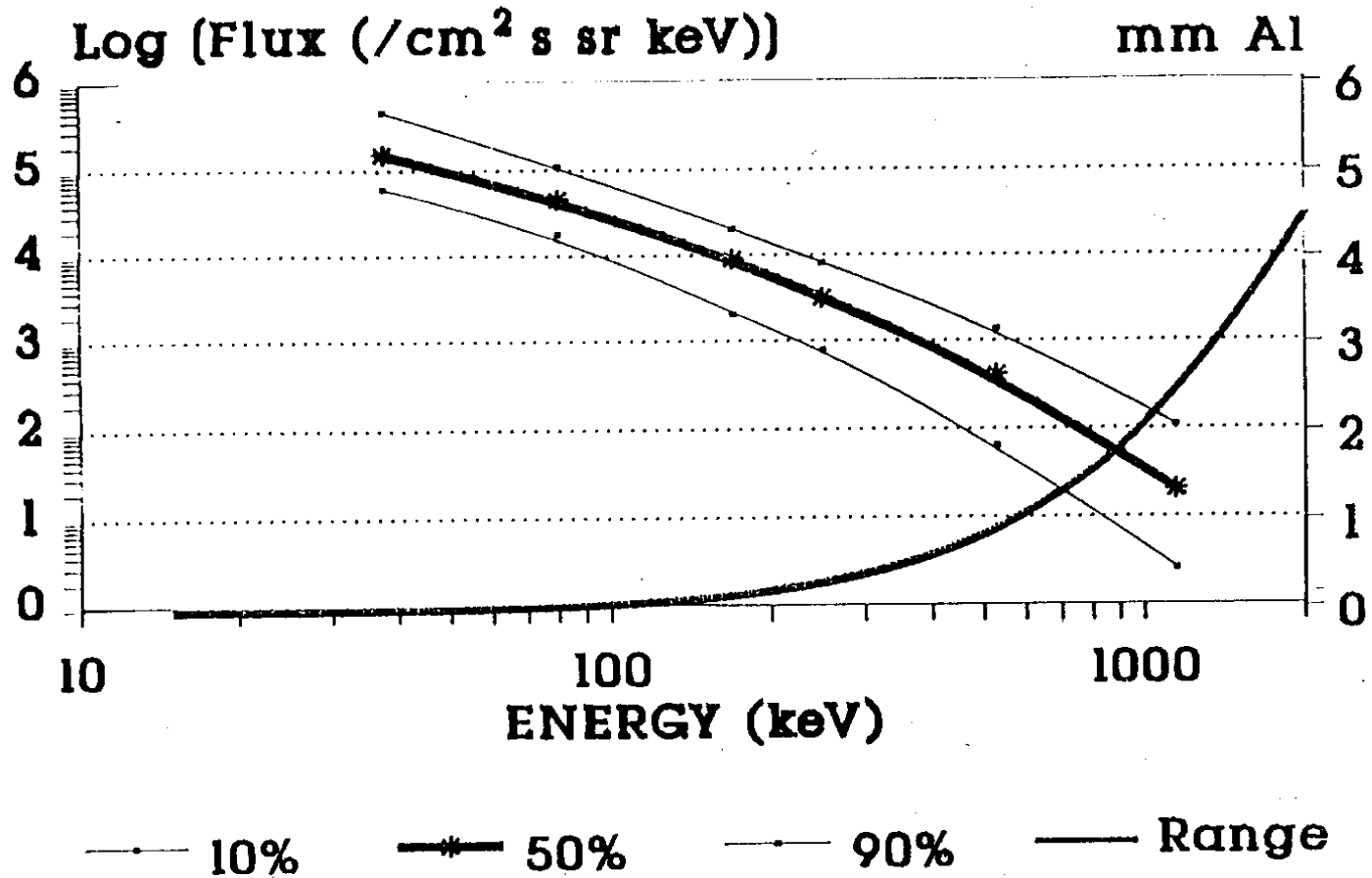


FIG 4

RAE_SPSM

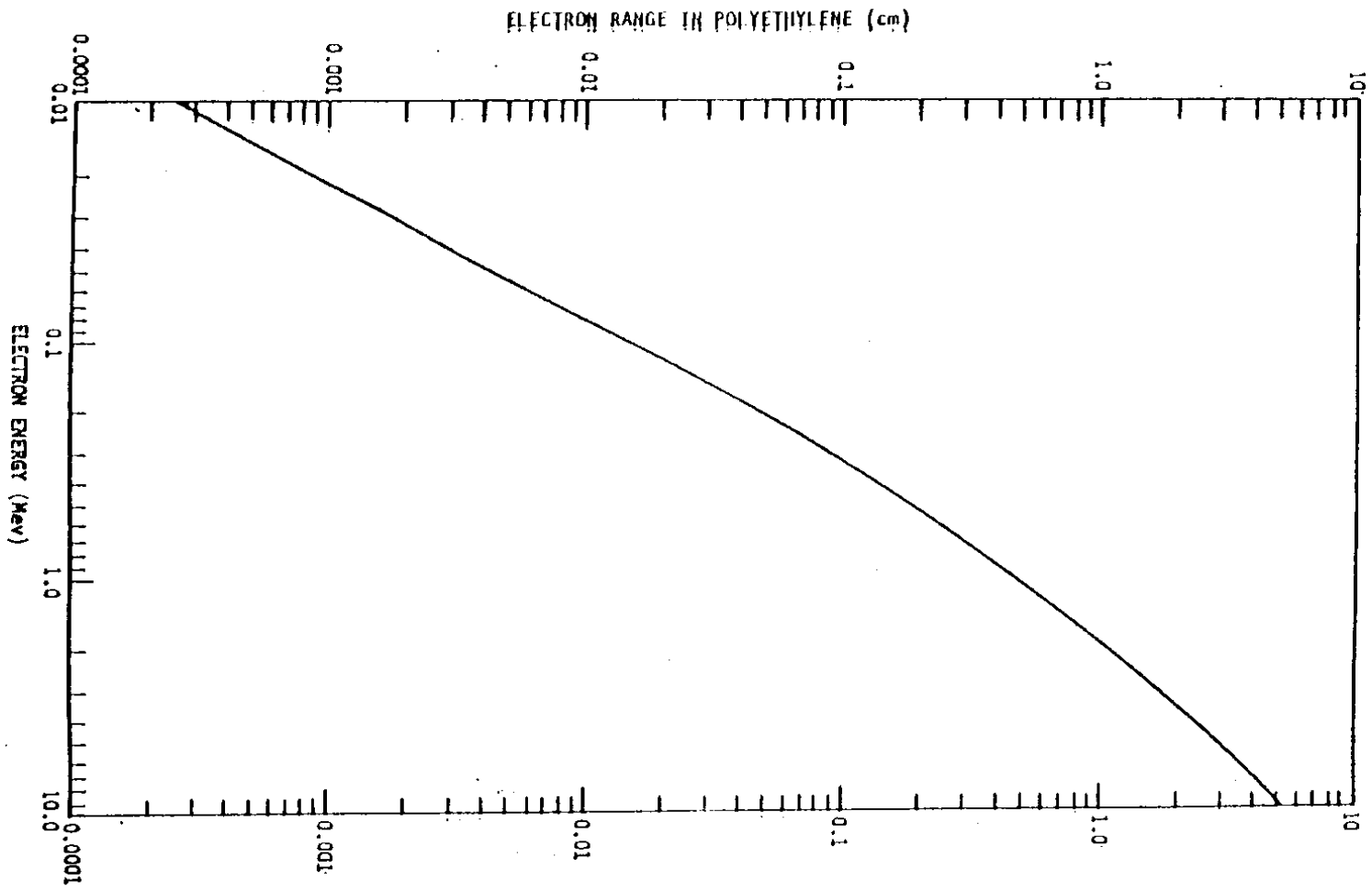
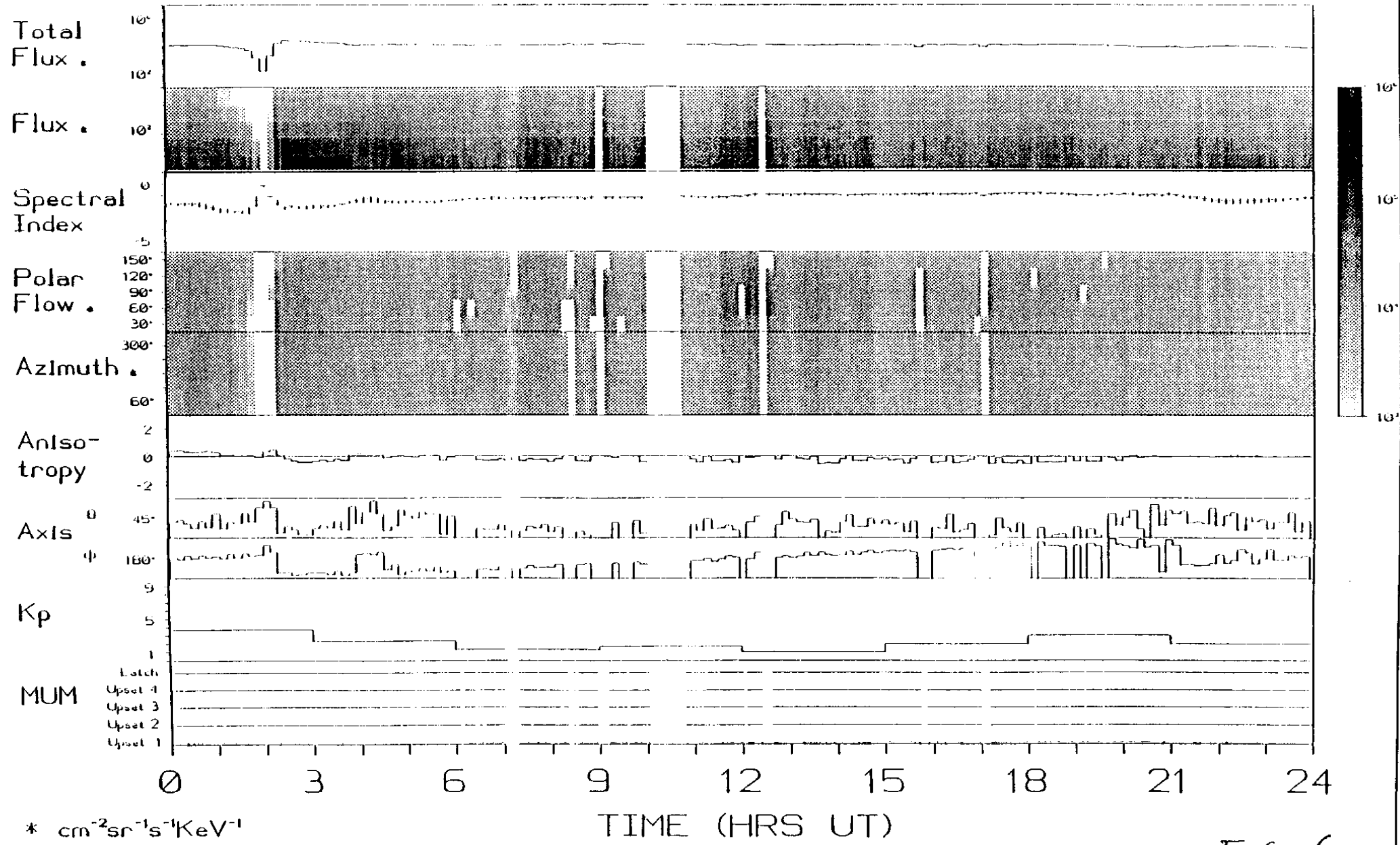


Figure 5

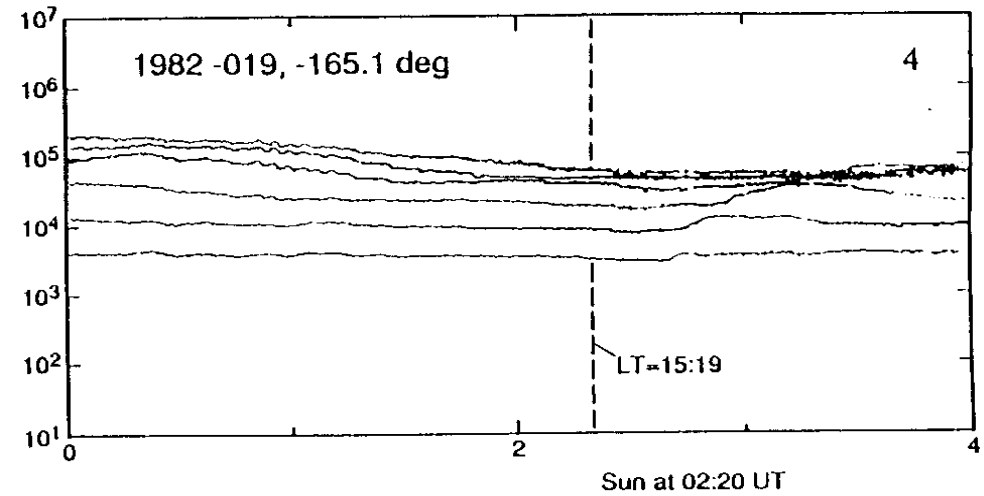
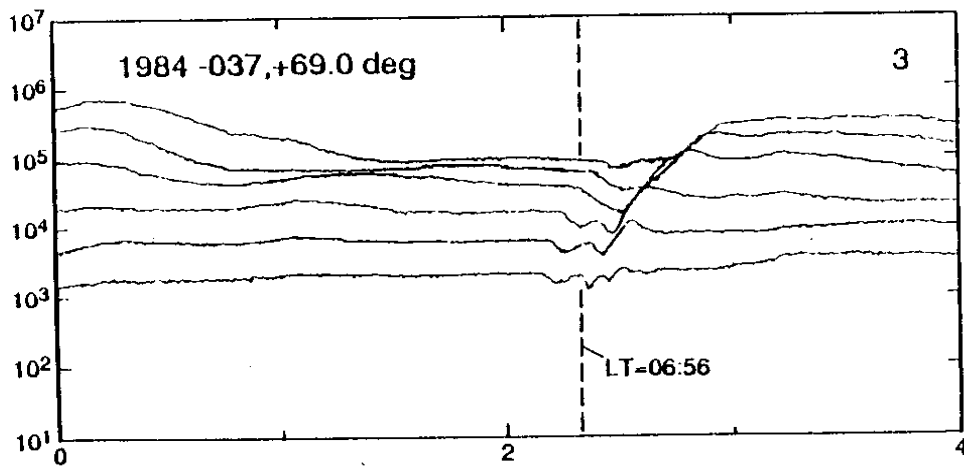
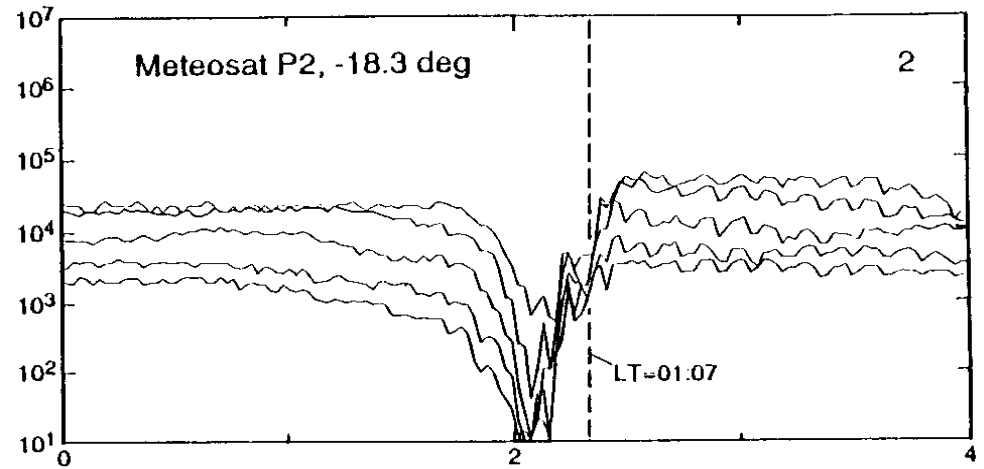
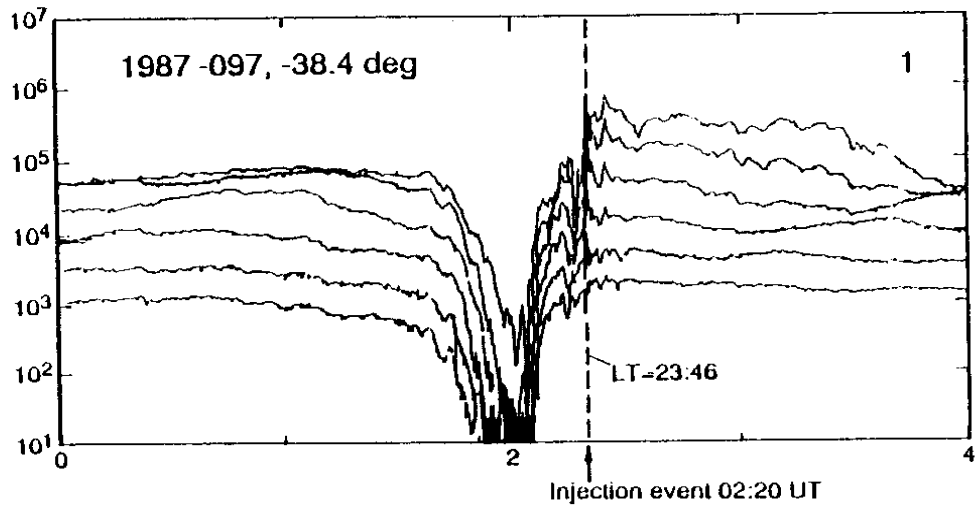
METEOSAT-P2 Space Environment Monitor
 DAILY SUMMARY FOR DAY 179 (27 JUN) 1988



* $\text{cm}^{-2} \text{sr}^{-1} \text{s}^{-1} \text{KeV}^{-1}$

TIME (HRS UT)

FIG 6



Time (UT)
27 JUNE, 1988

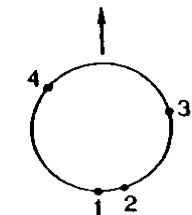
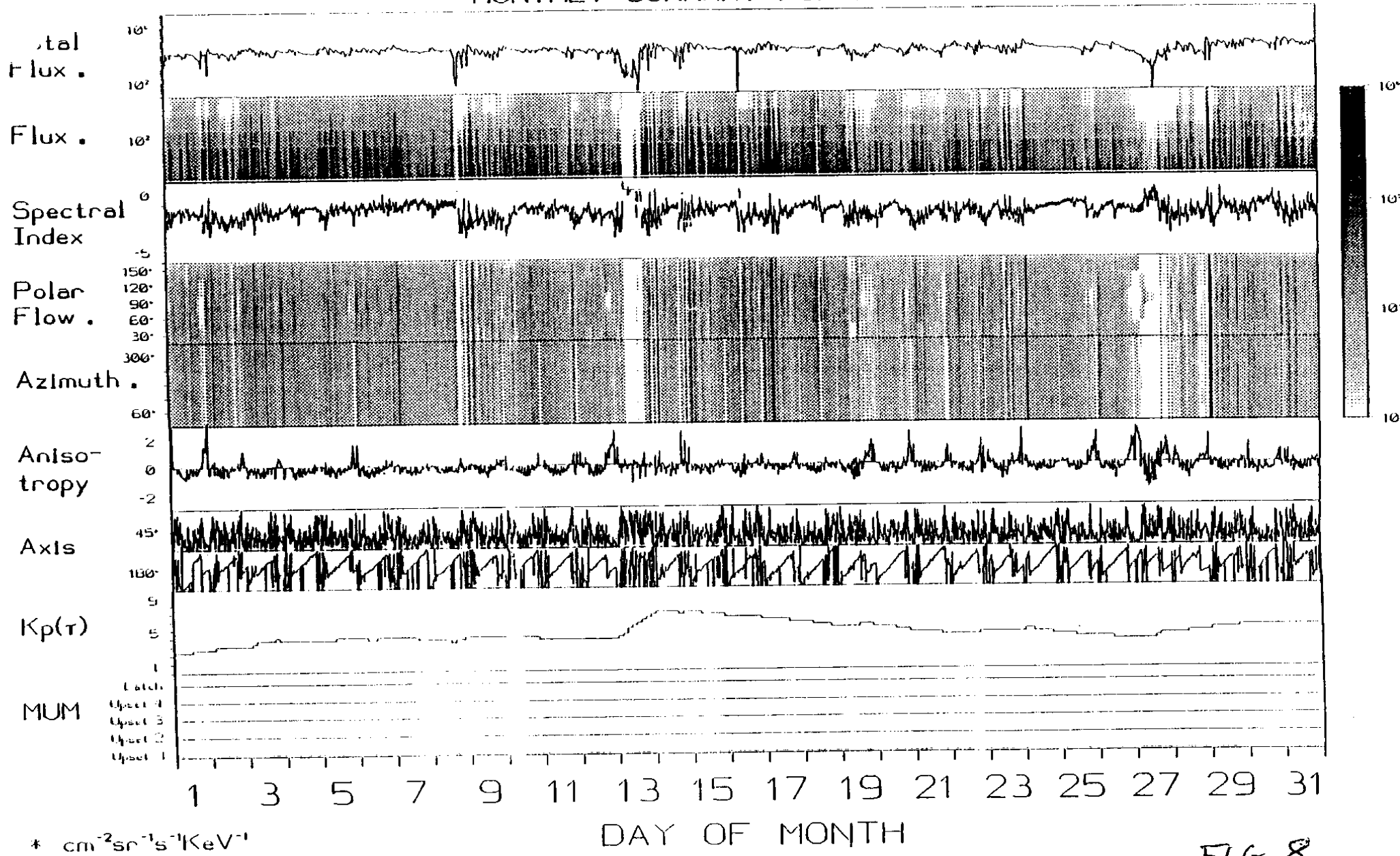


FIG 7

METEOSAT-P2 Space Environment Monitor
 MONTHLY SUMMARY FOR MAR 1989



* $\text{cm}^{-2}\text{sr}^{-1}\text{s}^{-1}\text{KeV}^{-1}$

FIG 8

july 1988 to june 1989

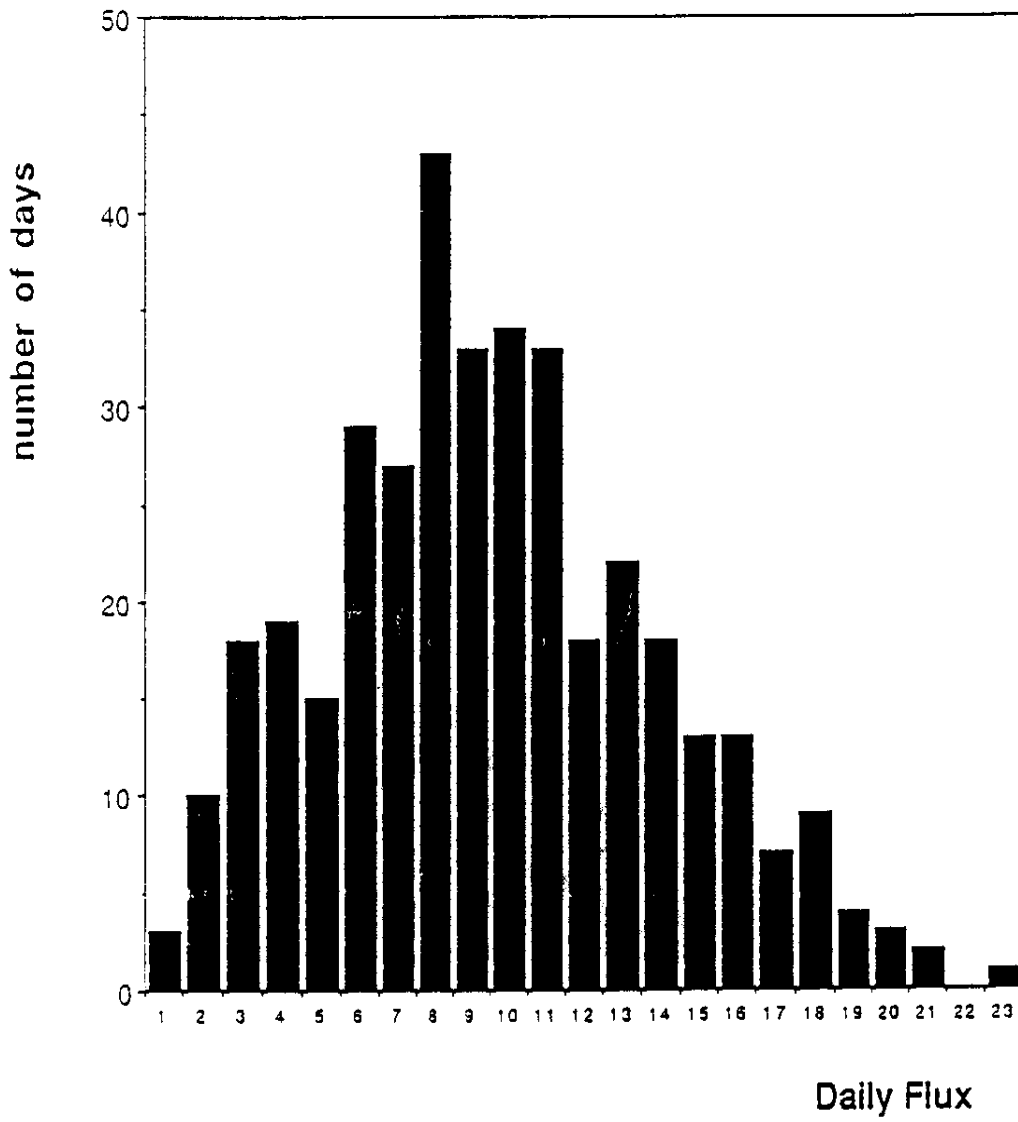


FIG 10

July 1988 to June 1989

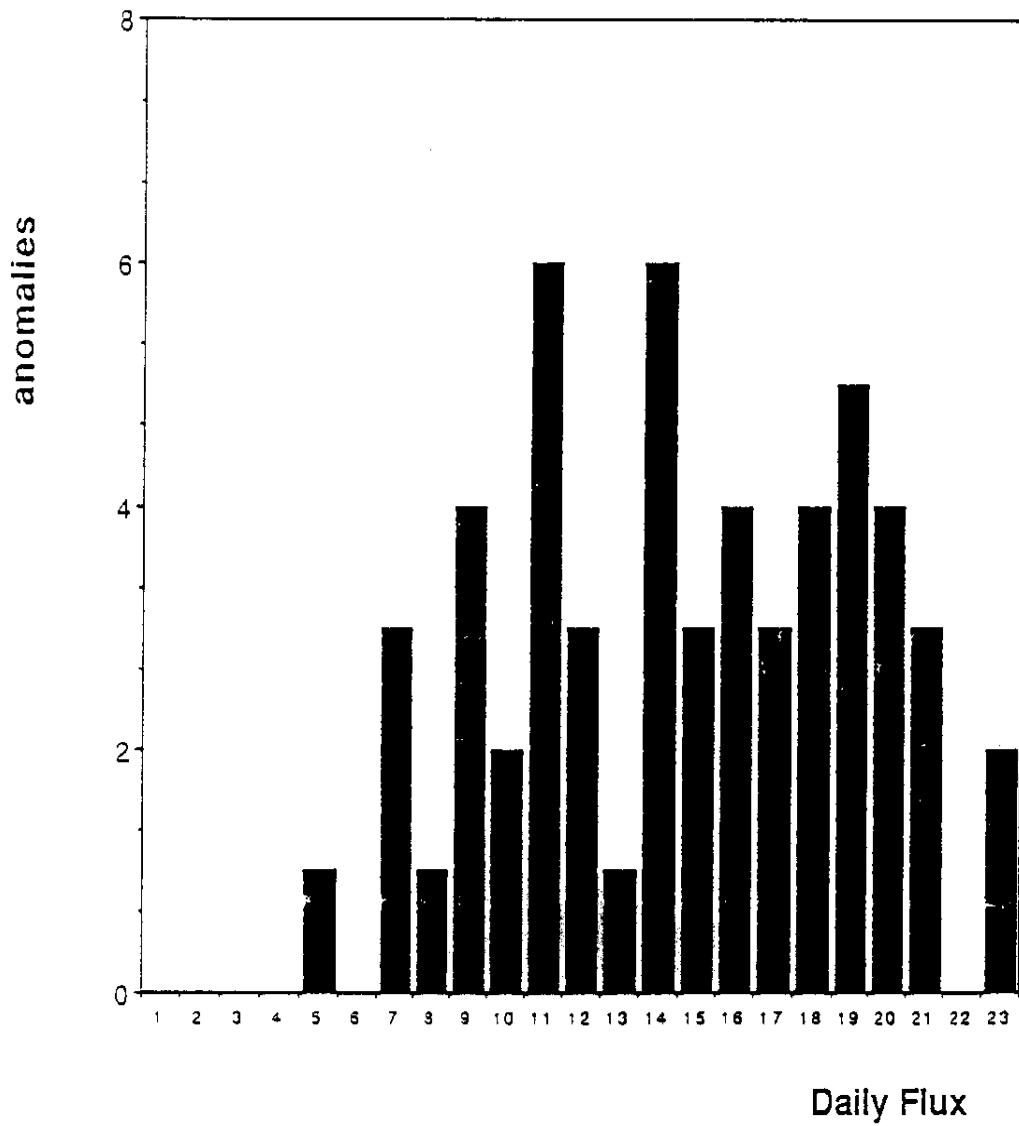


FIG 11

July 1988 to June 1989

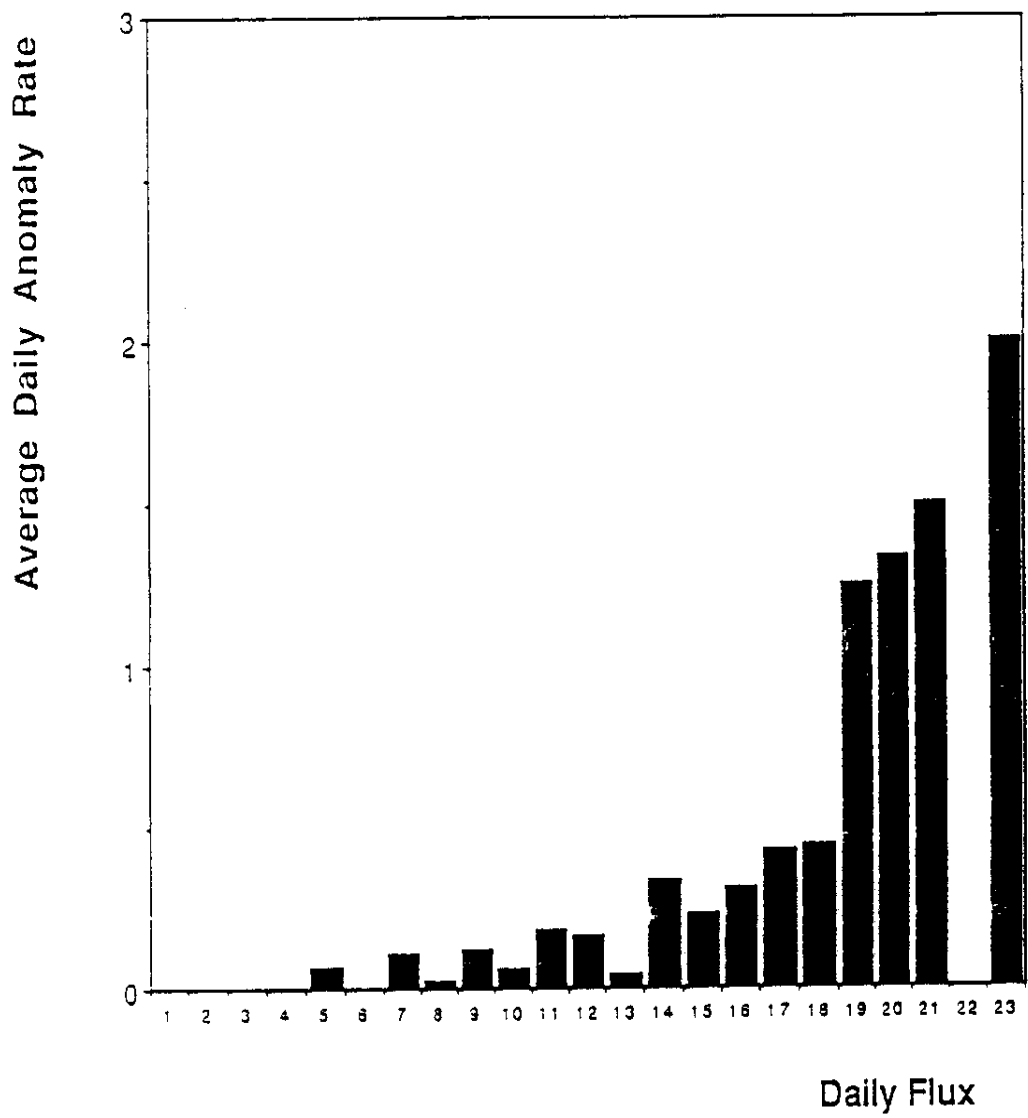


FIG 12

July 1988 to June 1989

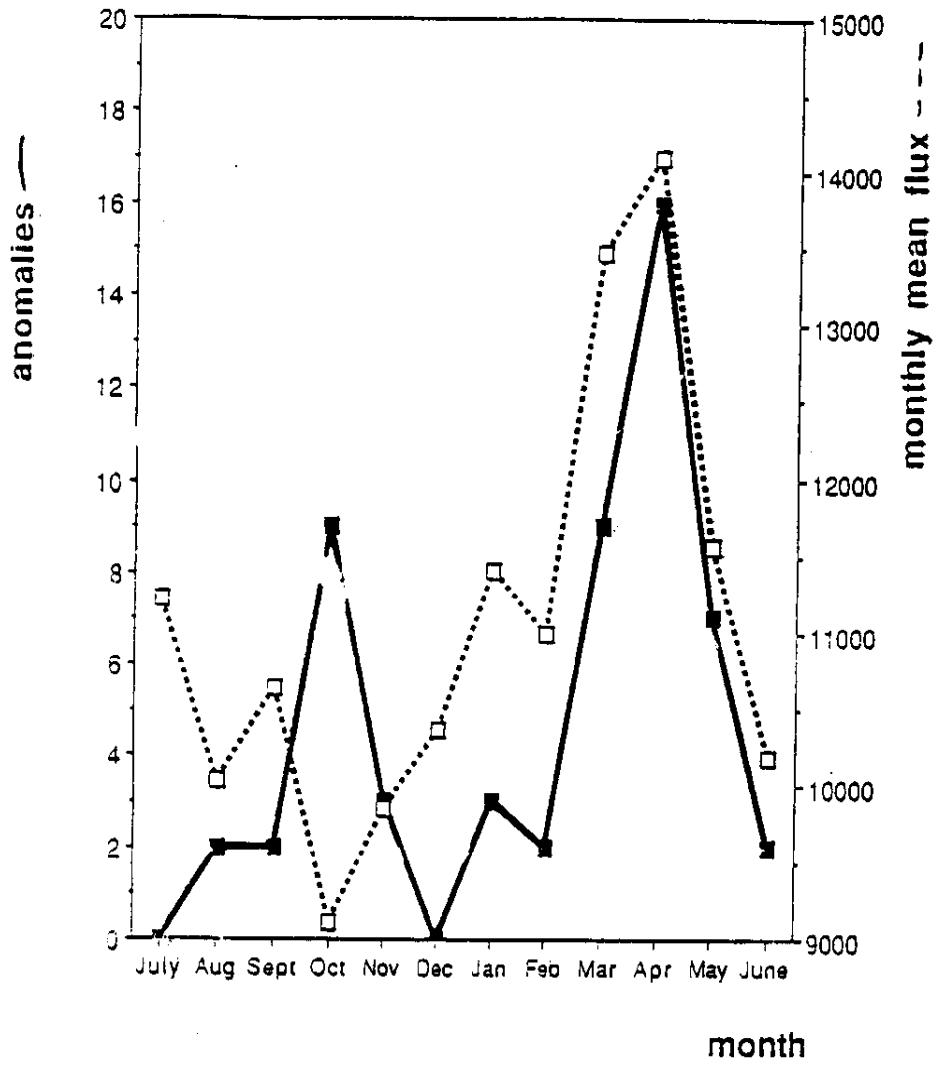


FIG 13

DUMP OF TAPE JRUTC2

INPUT TAPE JRUTC2 ON HT1
 DATA INPUT H9 NF=91 SR=2 1 1 SR=89 LAST 1

D-80282

FILE	INPUT RECS.	DATA INPUT	RECORDS INPUT	MAX. SIZE	READ ERROR SUMMARY				INPUT RETRIES	
1	5	5	80	0	0	0	0	0	0	
FILE	2	REC ORD	1	LENGTH	2048BYTES					
(0)	00000000	00000000	8547AE40	AE46A86F	0D4756DD	CC47953F	2248E083	36481E61	BDC01BA2	523F67D6
(4)	3848AD92	00000000	00000000	00000000	00000000	00000000	00000000	00000000	00000000	00000000
(8)	00000000	00000000	00000000	00000000	00000000	00000000	00000000	00000000	00000000	00000000
(12)	00000000	00000000	00000000	00000000	00000000	00000000	00000000	00000000	00000000	00000000
(16)	00000000	00000000	00000000	00000000	00000000	00000000	00000000	00000000	00000000	00000000
(20)	00000000	00000000	00000000	00000000	00000000	00000000	00000000	00000000	00000000	00000000
(24)	00000000	00000000	00000000	00000000	00000000	00000000	00000000	00000000	00000000	00000000
(28)	00000000	00000000	00000000	00000000	00000000	00000000	00000000	00000000	00000000	00000000
(32)	00000000	00000000	00000000	00000000	00000000	00000000	00000000	00000000	00000000	00000000
(36)	00000000	00000000	00000000	00000000	00000000	00000000	00000000	00000000	00000000	00000000
(40)	2A476295	E547FA62	5D4803DE	8A488FE3	EAC6E358	3E3F1967	43489260	65483B97	5A4856C9	53486895
(44)	3F489BC6	00000000	00000000	00000000	00000000	00000000	00000000	00000000	00000000	00000000
(48)	00000000	00000000	00000000	00000000	00000000	00000000	00000000	00000000	00000000	00000000
(52)	00000000	00000000	00000000	00000000	00000000	00000000	00000000	00000000	00000000	00000000
(56)	00000000	00000000	00000000	00000000	00000000	00000000	00000000	00000000	00000000	00000000
(60)	00000000	00000000	00000000	00000000	00000000	00000000	00000000	00000000	00000000	00000000
(64)	00000000	00000000	00000000	00000000	00000000	00000000	00000000	00000000	00000000	00000000
(68)	00000000	00000000	00000000	00000000	00000000	00000000	00000000	00000000	00000000	00000000
(72)	00000000	00000000	00000000	00000000	00000000	00000000	00000000	00000000	00000000	00000000
(76)	A8420000	F8420000	0F3FA52A	9D3FB67B	AA47A777	BB461502	53471D11	F24770A7	5648C07E	7348282C
(80)	C8C99009	3F3FD08E	4F4871FB	72481A32	8C485D01	6E482398	CF486FFB	00000000	00000000	00000000
(84)	00000000	00000000	00000000	00000000	00000000	00000000	00000000	00000000	00000000	00000000
(88)	00000000	00000000	00000000	00000000	00000000	00000000	00000000	00000000	00000000	00000000
(92)	00000000	00000000	00000000	00000000	00000000	00000000	00000000	00000000	00000000	00000000
(96)	00000000	00000000	00000000	00000000	00000000	00000000	00000000	00000000	00000000	00000000
(100)	00000000	00000000	00000000	00000000	00000000	00000000	00000000	00000000	00000000	00000000
(104)	00000000	00000000	00000000	00000000	00000000	00000000	00000000	00000000	00000000	00000000
(108)	00000000	00000000	00000000	00000000	00000000	00000000	00000000	00000000	00000000	00000000
(112)	00000000	00000000	00000000	24440000	8C410000	3C430000	A8430000	F8430000	9D3FB67B	E53F0911
(116)	A2476610	88465803	4B471548	ED471BC4	59480E6E	60488677	D9C004C7	8A3FCF45	53486895	45488D2D
(120)	53486895	614844FD	5A4856C9	00000000	00000000	00000000	00000000	00000000	00000000	00000000
(124)	00000000	00000000	00000000	00000000	00000000	00000000	00000000	00000000	00000000	00000000
(128)	00000000	00000000	00000000	00000000	00000000	00000000	00000000	00000000	00000000	00000000
(132)	00000000	00000000	00000000	00000000	00000000	00000000	00000000	00000000	00000000	00000000
(136)	00000000	00000000	00000000	00000000	00000000	00000000	00000000	00000000	00000000	00000000
(140)	00000000	00000000	00000000	00000000	00000000	00000000	00000000	00000000	00000000	00000000
(144)	00000000	00000000	00000000	00000000	00000000	00000000	00000000	00000000	00000000	00000000
(148)	00000000	00000000	00000000	00000000	00000000	00000000	00000000	00000000	00000000	00000000
(152)	C0410000	84430000	FC430000	3A440000	E53F0811	15402E53	9C4741D0	6F465305	38473F40	F84798C3
(156)	5648C078	4A482D05	DEC01F73	A83F8018	55486462	484883C7	33488A2B	53486895	65483B97	00000000
(160)	00000000	00000000	00000000	00000000	00000000	00000000	00000000	00000000	00000000	00000000
(164)	00000000	00000000	00000000	00000000	00000000	00000000	00000000	00000000	00000000	00000000
(168)	00000000	00000000	00000000	00000000	00000000	00000000	00000000	00000000	00000000	00000000
(172)	00000000	00000000	00000000	00000000	00000000	00000000	00000000	00000000	00000000	00000000
(176)	00000000	00000000	00000000	00000000	00000000	00000000	00000000	00000000	00000000	00000000
(180)	00000000	00000000	00000000	00000000	00000000	00000000	00000000	00000000	00000000	00000000
(184)	00000000	00000000	00000000	00000000	00000000	00000000	00000000	00000000	00000000	00000000
(188)	00000000	00000000	00000000	00000000	00000000	00000000	00000000	00000000	00000000	00000000
(192)	5E5E5E5E	5E5E5E5E	5E5E5E5E	5E5E5E5E	5E5E5E5E	5E5E5E5E	5E5E5E5E	5E5E5E5E	5E5E5E5E	5E5E5E5E
(196)	5E5E5E5E	5E5E5E5E	5E5E5E5E	5E5E5E5E	5E5E5E5E	5E5E5E5E	5E5E5E5E	5E5E5E5E	5E5E5E5E	5E5E5E5E
(200)	5E5E5E5E	5E5E5E5E	5E5E5E5E	5E5E5E5E	5E5E5E5E	5E5E5E5E	5E5E5E5E	5E5E5E5E	5E5E5E5E	5E5E5E5E
(204)	5E5E5E5E	5E5E5E5E	5E5E5E5E	5E5E5E5E	5E5E5E5E	5E5E5E5E	5E5E5E5E	5E5E5E5E	5E5E5E5E	5E5E5E5E

FILE	RECS.	INPUT	SIZE	PERM	ZERO	B	SHORT	UNDEF.	#RECS.	TOTAL#
	2	962	2048	0	0	0	0	0	0	0
FILE	89	RECORD	289	LENGTH	384 BYTES					
(0)	00000000	00000000	00000000	00000000	00000000	00000000	00000000	00000000	00000000	00000000
(40)	00000000	00000000	00000000	00000000	00000000	00000000	00000000	00000000	00000000	00000000
(80)	00000000	00000000	00000000	00000000	00000000	00000000	00000000	00000000	00000000	00000000
(120)	00000000	00000000	00000000	00000000	00000000	00000000	00000000	00000000	00000000	00000000
(160)	00000000	00000000	00000000	00000000	00000000	00000000	00000000	00000000	00000000	00000000
(200)	00000000	00000000	00000000	00000000	00000000	00000000	00000000	00000000	00000000	00000000
(240)	00000000	00000000	00000000	00000000	00000000	00000000	00000000	00000000	00000000	00000000
(280)	00000000	00000000	00000000	00000000	00000000	00000000	00000000	00000000	00000000	00000000
(320)	00000000	00000000	00000000	00000000	00000000	00000000	00000000	00000000	00000000	00000000
(360)	00000000	00000000	00000000	00000000	00000000	00000000	00000000	00000000	00000000	00000000

FILE	INPLT	DATA RECORDS	MAX.	READ ERROR SUMMARY				INPUT RETRIES		
	RECS.	INPUT	SIZE	PERM	ZERO	3	SHORT	UNDEF.	#RECS.	TOTAL#
89	289	290	2048	0	0	0	0	0	0	0

EOJ DUMP STOPPED AFTER FILE 9 # OF PERMANENT READ ERRORS 0

START TIME 09/22/90 11:13:09 STOP TIME 09/22/90 11:17:41

DUMP OF TAPE JROUTC2

INPUT TAPE JROUTC2 ON HT1
DATA INPUT H9 NF=90 SR=2=LAST=1 SR=89=1 1

FILE	INPUT RECS.	DATA RECORDS INPUT	MAX. SIZE	READ ERROR SUMMARY	INPUT RETRIES
1	5	5	80	PERM ZERO B SHCRT UNDEF.	#RECS. TOTAL#
FILE	2 RECORD	962 LENGTH	384BYTES		
(0)	334589E1	334545EC 3A47D412	0047B713	ED462898 3947A80B	B147697E F347282C 75C0E85D 363F69B7
(4)	0E489841	1F48EC5C F34716FF	1B48F6C2	93484B35 BC46E0DF	C34621C7 B746A6C6 B4467327 B746C64F
(8)	C446BEE1	8146770D A4466D66	C346C670	0046C876 D246E6AE	CA462619 D346EF18 0447F90F BD462013
(12)	BD462013	BD46893D D246E9AE	B2463B45	A146344B 8A465686	A2461AE9 8E465E4F B746428E
(16)	B74619CA	C846DC1C D246E9AE	D246E9AE	C7462EA5 F246BC65	CD46F847 C34628BA 64466D8E 8F46690A
(20)	E54612AC	00000000 00000000	00000000	00000000 00000000	00000000 00000000 00000000 00000000
(24)	00000000	00000000 00000000	00000000	00000000 00000000	00000000 00000000 00000000 00000000
(28)	00000000	00000000 00000000	00000000	00000000 00000000	00000000 00000000 00000000 00000000
(32)	00000000	00000000 00000000	00000000	00000000 00000000	963ED6F1 2A43BD23 52449076 00000000
(36)	00000000	E1440080 30420000	F2430000	67440000 AA440080	

FILE	INPUT RECS.	DATA RECORDS INPUT	MAX. SIZE	READ ERROR SUMMARY	INPUT RETRIES
2	962	963	2048	PERM ZERO B SHCRT UNDEF.	#RECS. TOTAL#
FILE	89 RECORD	1 LENGTH	2048BYTES		
(0)	00000000	00400000 A14625E6	7A450000	DB45BACD D3468180	8047DA67 97472B0C 05C128FB 783F5663
(4)	7E471D20	4B47FC7A F34617FF	37472FAC	86473BB7 FD4531A6	FF4539B5 0946D6F7 F7453B13 F74521C8
(8)	0246BD19	B745B952 26460DC7	404629C6	3B46C0FB 09466C06	A6453EC9 B545E878 EC450663 3546DD0C
(12)	2E46C2E1	09460AD8 E3455562	B34555EC	8D45C85F E1453CDC	B045FFD5 9D45A25D C345FAB0 22461173
(16)	FA45D920	D045261B 934552B6	0745C4B1	2B463536 47466850	1E462C8C C645EE10 B945D018 1E462A0E
(20)	3E46315C	00000000 00000000	00000000	00000000 00000000	00000000 00000000 00000000 00000000
(24)	00000000	00000000 00000000	00000000	00000000 00000000	00000000 00000000 00000000 00000000
(28)	00000000	00000000 00000000	00000000	00000000 00000000	00000000 00000000 00000000 00000000
(32)	00000000	00000000 00000000	00000000	00000000 00000000	1D4091C6 CD42A5EC 384429F8 00000000
(36)	00000000	24440000 80410000	30430000	A8430000 F8430000	00400000 80400000 A0462C39 7A450000
(40)	B245A82F	8546F9B8 7A4747C0	DC47301A	14C1CAB9 633F170B	37475B5F 2C477591 C2463F2D 2D47C8CA
(44)	844706A7	EA45D89C E945415A	F245FC19	E4458FCF E44541D7	ED451C38 BA4537A2 2046051D 284680F6
(48)	27468B05	D54575EA 8C45C1DB	9745DCAD	C845A4AE 1B467D3A	2046EA8B 05463710 B1459F06 8A451BA7
(52)	984554F1	AA455E06 984507DC	A7452307	A345ACDD 22460AAC	C4452578 A9453AC5 99459143 EA45285D
(56)	414665BA	374678F8 14460B37	DE45F853	B545E94A 03468B62	1E46D871 00000000 00000000 00000000
(60)	00000000	00000000 00000000	00000000	00000000 00000000	00000000 00000000 00000000 00000000
(64)	00000000	00000000 00000000	00000000	00000000 00000000	00000000 00000000 00000000 00000000
(68)	00000000	00000000 00000000	00000000	00000000 00000000	00000000 00000000 00000000 00000000
(72)	00000000	00000000 114068B0	92425D6E	32442C62 00000000	00000000 5A44ABAA AA41ABAA 6A43ABAA
(76)	E0430000	25445555 80400000	C0400000	D146E90A 7A450000	CE45F588 AE4674E0 9C47C0BE 1E489E87
(80)	21C156CD	3D3FF4A0 5247BFBF	80476573	1347B75B 55476362	90473CA8 0F46E570 0346CE82 14461CC4
(84)	12461EC6	0C466F35 1346A586	EA4563A7	204663C8 19464AA0	2D466100 0E46293D 014668F8 0746CC59
(88)	1946A44E	514698EC 49460035	1A46EA34	0D462FCC D74537B3	D245A84B F44585B3 DA4535D3 CC45155D
(92)	D9455408	304631C3 FC45D332	F545677E	EC45C0B2 0F46F97B	41465F8E 34462D23 18468F37 0745B32E
(96)	034637E6	1E4691EE 234618CA	00000000	00000000 00000000	00000000 00000000 00000000 00000000
(100)	00000000	00000000 00000000	00000000	00000000 00000000	00000000 00000000 00000000 00000000
(104)	00000000	00000000 00000000	00000000	00000000 00000000	00000000 00000000 00000000 00000000
(108)	00000000	00000000 00000000	00000000	00000000 00000000	00000000 00000000 00000000 00000000
(112)	2E443C4B	00000000 00000000	5A44ABAA	AA41ABAA 6A43ABAA	E0430000 25445555 C0400000 00410000
(116)	E5464005	7A450000 A7456C51	844632B1	AD477355 3948AF50	2BC1E3F9 8C3F4362 4C47189B 7947A89F
(120)	4C477B61	5E474D63 7E471E20	18462793	194659F0 1F46EA46	14460FA6 1B468367 174645E5 0346EA15
(124)	1546C0C4	1046A2A9 15467D45	19464B00	07467DFD 22465CF5	2246A763 454648DA 2C468A2E 1E4616C4
(128)	2246E520	12467411 11468DE8	1646400C	124696C5 1646F4AD	14460A90 1B4680A8 1F460824 1A4635D0
(132)	1046F06E	1E4612DA 2B462620	27468329	1846BE7C 15463102	0246B995 1B4628B9 0D46C2C9 00000000
(136)	00000000	00000000 00000000	00000000	00000000 00000000	00000000 00000000 00000000 00000000
(140)	00000000	00000000 00000000	00000000	00000000 00000000	00000000 00000000 00000000 00000000
(144)	00000000	00000000 00000000	00000000	00000000 00000000	00000000 00000000 00000000 00000000
(148)	00000000	00000000 00000000	00000000	8E3E0202 3443B8CA	3E44D405 00000000 00000000 61440080

(152)	B0410000	72430000	E7430000	2A440080	00410000	20410000	2F47D03F	7A450000	0F462B75	1E4716CF
(156)	14483B38	734E1054	35C1F657	463F7829	C9472061	C047EDF9	994790CF	AC477591	C84784C7	65460B98
(160)	5E463579	6646CF37	5546578C	6A4671C0	6D46AB4F	3C46CF51	66465C76	874657C0	8146539F	AF46E72B
(164)	83469892	6C4610F1	7446A784	9A4661E7	88464138	8D46B5FE	87460307	4346E5D7	43463033	4D46BF70
(168)	424684F2	38462009	42467308	94465296	4D46CB60	49466C3D	414681F9	37466396	5346738E	6546BBB0
(172)	5C46089F	2546668C	14468512	2C467789	774633C1	00000000	00000000	00000000	00000000	00000000
(176)	00000000	00000000	00000000	00000000	00000000	00000000	00000000	00000000	00000000	00000000
(180)	00000000	00000000	00000000	00000000	00000000	00000000	00000000	00000000	00000000	00000000
(184)	00000000	00000000	00000000	00000000	00000000	00000000	00000000	00000000	00000000	00000000
(188)	573F60EC	C142F008	58447CB9	00000000	00000000	5A44ABAA	AA41ABAA	6A43ABAA	E0430000	25445555
(192)	5E5E5E5E									
(196)	5E5E5E5E									
(200)	5E5E5E5E									
(204)	5E5E5E5E									

FILE	INPUT RECS.	DATA RECORDS INPUT	MAX. SIZE	READ ERROR SUMMARY				INPUT RETRIES	
				PERM	ZERO	B	SHORT	UNDEF.	#RECS. TOTAL#
89	289	289	2048	0	0	0	0	0	0

EQJ DUMP STOPPED AFTER FILE 90 # OF PERMANENT READ ERRORS 0

START TIME 09/22/90 11:18:52 STOP TIME 09/22/90 11:22:41